AECL-7911

ATOMIC ENERGY OF CANADA LIMITED

L'ÉNERGIE ATOMIQUE DU CANADA LIMITÉE

NUMERICAL SIMULATION OF MODERATOR FLOW AND TEMPERATURE DISTRIBUTIONS IN A CANDU REACTOR VESSEL

Simulation numérique de la répartition des écoulements et des températures du modérateur dans une cuve de réacteur CANDU

L.N. CARLUCCI

Presented at the International Symposium on Refined Modelling of Flows held in Paris, France, 1982 September 7-10.

Chalk River Nuclear Laboratories Laboratoires nucléaires de Chalk River

Chalk River, Ontario

October 1982 octobre

ATOMIC ENERGY OF CANADA LIMITED

NUMERICAL SIMULATION OF MODERATOR FLOW AND TEMPERATURE DISTRIBUTIONS IN A CANDU REACTOR VESSEL

by

L.N. Carlucci

Presented at the International Symposium on Refined Modelling of Flows held in Paris, France, 1982 September 7-10.

Printed with permission from the conference organizers.

Chalk River Nuclear Laboratories
Chalk River, Ontario K0J 1J0
1982 October

AECL-7911

L'ENERGIE ATOMIQUE DU CANADA, LIMITEE

Simulation numérique de la répartition des écoulements et des températures du modérateur dans une cuve de réacteur CANDU

par

L.N. Carlucci

Résumé

On décrit, dans ce rapport, les prédictions numériques des deux champs bidimensionnels d'écoulement et de température d'un liquide intérieurement chauffé dans une cuve typique de réacteur CANDU. Le moment de turbulence et le transport de l'énergie sont simulés au moyen du modèle k-ε. Les résultats obtenus à l'état stable et en conditions transitoires font l'objet de commentaires. Les représentations analogiques du volume de contrôle fini des équations de conservation sont résolues au moyen d'une version modifiée du code TEACH.

Laboratoires nucléaires de Chalk River
Chalk River, Ontario K0J 1J0

Octobre 1982

AECL-7911

ATOMIC ENERGY OF CANADA LIMITED

NUMERICAL SIMULATION OF MODERATOR FLOW AND TEMPERATURE DISTRIBUTIONS IN A **CANDU** REACTOR VESSEL

by

L.N. Carlucci

ABSTRACT

This paper describes numerical predictions of the two-dimensional flow and temperature fields of an internally-heated liquid in a typical CANDU reactor vessel. Turbulence momentum and energy transport are simulated using the k-ε model. Both steady-state and transient results are discussed. The finite control volume analogues of the conservation equations are solved using a modified version of the TEACH code.

Chalk River Nuclear Laboratories
Chalk River, Ontario K0J 1J0
1982 October

AECL-7911

NUMERICAL SIMULATION OF MODERATOR FLOW AND TEMPERATURE DISTRIBUTIONS IN A CANDU REACTOR VESSEL

L.N. Carlucci
Atomic Energy of Canada Limited
Research Company
Chalk River Nuclear Laboratories
Chalk River, Ontario K0J 1J0

INTRODUCTION

A typical CANDU* reactor vessel (Figure 1) is filled with a matrix of approximately four hundred tubes containing nuclear fuel. High pressure primary coolant is circulated inside the tubes to remove the thermal energy generated by the fission reaction. The volume surrounding the tubes is filled with low pressure heavy water called the moderator. The function of the moderator is to slow down fast neutrons to "thermal speeds" so that the fission reaction can be maintained. In so doing, it absorbs a significant amount of thermal energy**. To remove this energy, the moderator is continually circulated through the reactor vessel and thence through external heat exchangers. The heavy water is pumped into the reactor through a series of nozzles mounted just below the horizontal mid-plane and is removed from the vessel through large pipes located near the bottom (see Figure 1).

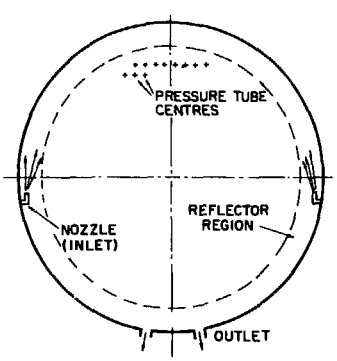

Figure 1

Simplified Front View of Reactor Vessel

---

* CANDU - CANada Deuterium Uranium

** This neutron and gamma ray heat load is approximately 120 MW in a typical 600 MWe reactor.

Knowledge of the moderator temperature and flow distributions at different reactor operating conditions is useful to both designers and safety analysts. Accordingly, a numerical model has been developed to simulate the steady-state and time-dependent behaviour of moderator flow in a typical CANDU reactor vessel. The code employs the k-ε model to simulate turbulent diffusion of momentum and energy, and porous media concepts to model the effect of the tube matrix on the flow distribution.

CONSERVATION EQUATIONS

The equations solved are those of radial and circumferential momentum, continuity, energy, turbulent kinetic energy and turbulence energy dissipation rate. They can be represented in the following general form, Patankar (1980):

$$\frac{\partial}{\partial t}(\beta\rho\phi) + \frac{1}{r}\frac{\partial}{\partial r}\left[r\beta(\rho v\phi - \Gamma_\phi \frac{\partial\phi}{\partial r})\right] + \frac{1}{r}\frac{\partial}{\partial\theta}\left[\beta(\rho u\phi - \Gamma_\phi \frac{\partial\phi}{r\partial\theta})\right] = \beta S_\phi \qquad (1)$$

where t is time, r and θ are the radial and circumferential coordinates, β is the volume-based porosity (local fluid-filled volume ÷ local total volume), ρ is the fluid density, u and v are the circumferential and radial velocities, φ is the general transport parameter, Γ_ϕ is the exchange coefficient and S_ϕ is the source term. Definitions of φ, Γ_ϕ and S_ϕ for each of the six conservation equations are given in Table 1 below.

TABLE 1: DEFINITION OF φ, Γ_ϕ AND S_ϕ FOR EQUATION (1)

EQUATION	φ	Γ_ϕ	S_ϕ
RADIAL MOMENTUM	v	μ_{eff}	$-\frac{\partial P}{\partial r} - \alpha\rho(T-T_r)g_r + \frac{\rho u^2}{r} - 2\mu_{eff}\frac{v}{r^2} + \frac{1}{r}\frac{\partial}{\partial r}(\mu_{eff}\frac{r\partial v}{\partial r}) + \frac{1}{r}\frac{\partial}{\partial\theta}\left[r\mu_{eff}\frac{\partial}{\partial r}(\frac{u}{r})\right] - \frac{2\mu_{eff}}{r^2}\frac{\partial u}{\partial\theta} - F_r$
CIRCUMFERENTIAL MOMENTUM	u	μ_{eff}	$-\frac{1}{r}\frac{\partial P}{\partial\theta} - \alpha\rho(T-T_r)g_\theta - \frac{\rho uv}{r} + \frac{\mu_{eff}}{r}(\frac{\partial u}{\partial r} + \frac{\partial v}{r\partial\theta} - \frac{u}{r}) + \frac{1}{r}\frac{\partial}{\partial r}\left[\mu_{eff}\, r(\frac{\partial v}{r\partial\theta} - \frac{u}{r})\right] + \frac{1}{r}\frac{\partial}{\partial\theta}\left[\frac{\mu_{eff}}{r}(\frac{\partial u}{\partial\theta} + 2v)\right] - F_\theta$
CONTINUITY	1	0	0
ENERGY	T	$\frac{\mu}{Pr} + \frac{\mu_t}{\sigma_t}$	$\frac{\Omega}{c_p}$
TURBULENT KINETIC ENERGY	k	$\frac{\mu_{eff}}{\sigma_k}$	$G_S + G_B - \varepsilon\rho$
ENERGY DISSIPATION RATE	ε	$\frac{\mu_{eff}}{\sigma_\varepsilon}$	$\frac{\varepsilon}{k}[C_1(G_S + G_B) - C_2\rho\varepsilon]$

$$G_S = \mu_{eff}\left\{2\left[\left(\frac{\partial v}{\partial r}\right)^2 + \left(\frac{1}{r}\frac{\partial u}{\partial\theta} + \frac{v}{r}\right)^2\right] + \left(\frac{\partial v}{r\partial\theta} + \frac{\partial u}{\partial r} - \frac{u}{r}\right)^2\right\} \quad ; \quad G_B = \alpha\frac{\mu_t}{\sigma_t}\left[g_\theta\frac{1}{r}\frac{\partial T}{\partial\theta} + g_r\frac{\partial T}{\partial r}\right]$$

Constants, Rodi (1980)

σ_t	σ_k	σ_ε	C_1	C_2	C_μ
0.9	1.0	1.3	1.44	1.92	0.09

The system governed by equation (1) and Table 1 is based on the following assumptions and simplifications:

- The flow and temperature fields are two-dimensional,
- The fluid is incompressible,
- The Boussinesq approximation is used to model buoyancy effects in the momentum equations,
- Viscous dissipation on the rate of energy transfer is neglected,
- Turbulence fluxes are modelled using the eddy viscosity concept. The eddy viscosity and diffusivity are functions of the turbulence kinetic energy and dissipation rate, Rodi (1980),
- The high Reynolds number version of the k-ε model is used. Near-wall effects are treated using suitably defined wall functions, Rodi (1980) and Gosman and Pun (1974),
- The buoyancy production/destruction of turbulence kinetic energy is included in the ε equation using the same empirical constant as for the shear production,
- The effect of the tube matrix on the flow is treated by utilizing the volume based porosity β to account for the flow volume reduction and by suitably defined friction factor correlations to account for the tube bundle anisotropic hydraulic impedance,
- Turbulence generation by the tubes is assumed negligible compared with that generated by the jets near the wall.

Boundary Conditions, Wall Functions and Heat Load

The system of equations having the general form (1) is elliptic and therefore conditions must be prescribed along the entire vessel boundary. The flow and temperature fields are assumed symmetric about a vertical plane that bisects the vessel. The solid adiabatic wall is modelled by setting $\partial T/\partial r = u = v$. At the vertical plane of symmetry, the circumferential velocity as well as all gradients are set to zero, i.e. $u = \partial T/r\partial\theta = \partial u/r\partial\theta = \partial k/r\partial\theta = \partial\varepsilon/r\partial\theta = 0$. Flow and turbulence conditions at the inlet nozzle are specified as follows:

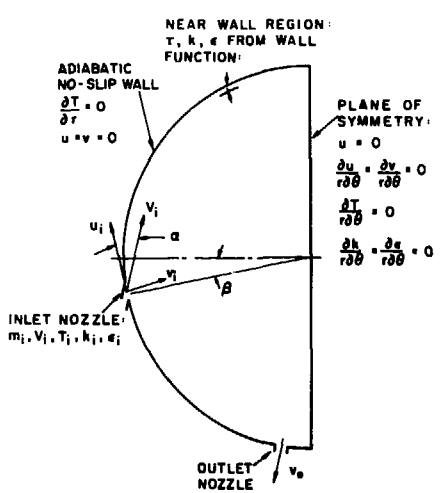

Figure 2

Two-Dimensional Idealization of Reactor Vessel Illustrating Boundary Conditions

$$u_i = V_i \cos \alpha \quad (2)$$

$$v_i = V_i \sin \alpha \quad (3)$$

$$k_i = 0.001\, V_i^2 \quad (4)$$

$$\varepsilon_i = k_i^{3/2}/A_n^{1/2} \quad (5)$$

where V_i is the inlet velocity at the nozzle and A_n is the nozzle area. The inlet turbulence conditions are somewhat arbitrary; however, they have a negligible effect on the state of turbulence within the vessel. Finally, the outlet velocity is specified such that the outlet flowrate is equal to the inlet flowrate.

The high Reynolds number version of the k-ε model is not applicable near the wall. Hence the wall function method is used to calculate the wall shear stress as well as the near-wall turbulence kinetic energy and corresponding dissipation rate.

The volumetric heat load resulting from neutron and gamma heating is specified by assuming it varies in proportion to the channel power in the core region and that it is constant in the reflector region. The resulting profile shape is illustrated in Figure 3.

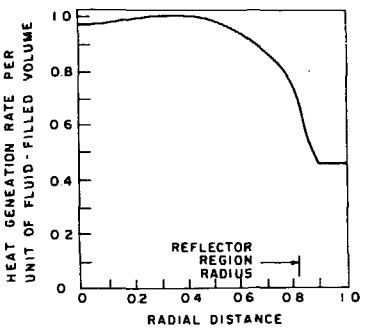

Figure 3

Normalized Volumetric Heat Load Distribution Based on Channel Power

FINITE CONTROL VOLUME EQUATIONS AND NUMERICAL SOLUTION

The method of discretization and solution procedure used are described in detail elsewhere (Patankar (1980), Gosman and Pun (1974)) so that only the salient features are given here. The region to be modelled is first subdivided into a number of control volumes using a polar coordinate grid (Figure 4). Each of the conservation equations is then integrated over its corresponding control volume. The resulting flux expressions are approximated using the hybrid upwind-central difference scheme. According to this scheme, convection terms at control volume faces are approximated using central differencing if the local Peclet number is less than two and upwind differencing if it is greater than two. The resulting discretized analogues of equation (1), for a control volume centered about a point p and surrounded by four neighbouring points nb is:

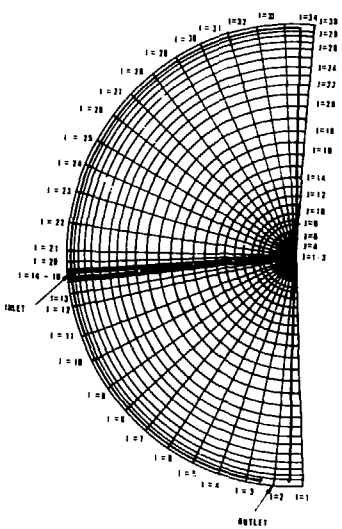

Figure 4

Typical Non-Uniform Grid Layout: 34 circumferential by 30 radial

$$(a_p + \rho VOL/\Delta t)\phi_p = \sum_{nb} a_{nb}\phi_{nb} + Su + \rho VOL\phi_p^o/\Delta t \qquad (6)$$

where a_p and a_{nb} are convection-diffusion coefficients, VOL is the cell volume, Δt is the time increment and the superscript o refers to the value of ϕ_p at the previous time step. Equation (6) is implicit in ϕ, hence it must be solved by iteration. This is accomplished by applying the tri-diagonal matrix algorithm on a line-by-line basis until the entire modelled region is covered. The same solution procedure is followed for each dependent variable in turn.

Equation (6) is used directly to solve for u,v,T,k and ε. The coupling between pressure and velocity is treated by solving a Poisson-like equation for pressure. Both the SIMPLE algorithm of Patankar and Spalding (1972) and the SIMPLER algorithm of Patankar (1980) have been used for this purpose. The former results in an equation for pressure correction while the latter results in an equation for pressure. Both equations have the same form as equation (6) and hence are solved in the same way.

For some steady-state non-isothermal simulations, improved convergence has been obtained by introducing an additional call of the SIMPLE algorithm directly after the solution of the energy equation. In these cases, the effect of density changes from one iteration to the next is incorporated directly into the pressure correction equation. For example, the radial velocity correction at point p required to satisfy continuity is defined by:

$$v' = \frac{1}{a_p}(A\,\Delta P' + g_r\,VOL\,\Delta\rho') \qquad (7)$$

where $\Delta P'$ is the required pressure correction difference and $\Delta\rho'$ is the change in the relative density from one iteration to the next.

Convergence and Computing Time

Convergence at steady-state or within a time step was deemed acceptable when the following criterion was satisfied for both momentum and mass conservation:

$$\left|R_{max}^{n} - R_{max}^{n-1}\right| \leq 5 \times 10^{-5} \qquad (8)$$

For momentum, R_{max} is defined as the maximum local residual divided by $a_p + \rho VOL/\Delta t$, hence it is effectively a velocity residual. For mass continuity R_{max} is defined as the maximum local divergence divided by the mean mass flow through the control volume. The number of iterations required to obtain a converged steady-state solution ranged from 300 for isothermal runs to several thousand for non-isothermal simulations. The CPU time required per iteration using a 34 circumferential by 30 radial grid was 1.2 s using SIMPLE and 1.8 s using SIMPLER on a CDC CYBER 170 Model 175 computer. Although the use of SIMPLER required fewer iterations to meet the above convergence criterion, the overall computing time to complete a run was roughly the same for the two methods.

RESULTS AND DISCUSSIONS

Isothermal Predictions

All isothermal simulations were done using the steady-state calculation procedure ($\Delta t = 10^{20}$). These runs were done to investigate the effects of grid

spacing, turbulence/no turbulence and tube matrix resistance on the predicted flow pattern.

The circumferential-radial grid configurations studied were 25 by 25, 34 by 30, 50 by 30 and 70 by 30. When turbulence was modelled, the predicted flow field was found to be grid-independent for all but the 25 by 25 grid. In contrast, when the turbulence model was suppressed*, the predicted flow field was found to be grid-dependent for all four grids tested. On the basis of these observations, all subsequent runs with turbulence simulated were done using the 34 by 30 grid (Figure 4).

The optimum tube bank resistance coefficient was established by comparing the predicted isothermal flow field with that measured. The experimental results of Hepworth (1967) were used for this purpose. These were conducted with a full size half-cylinder mock-up of a reactor vessel, complete with tube matrix. Figures 5(a) and 5(b) compare the predicted and measured flow patterns. The shape and extent of the recirculation region above the horizontal mid-plane is predicted quite well. Predicted velocity magnitudes and the location of the near-wall stagnation point are also in good agreement with those measured. A decrease in the optimized tube bank resistance coefficient results in a shift of the stagnation point location towards the outlet and in a shift of the vortex center towards the center of the top half of the vessel.

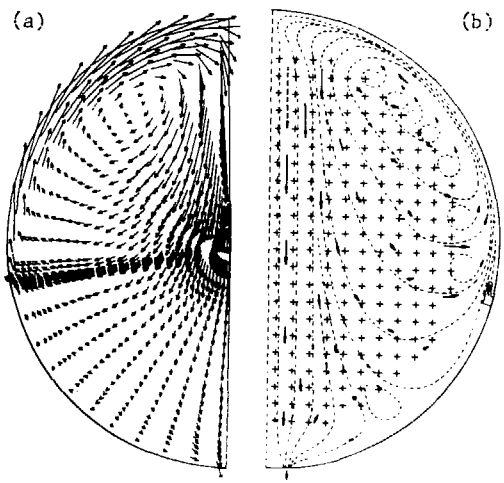

Figure 5

Isothermal Velocity Fields. (a) Predicted, (b) Measured

Non-Isothermal Predictions

The nature of the flow pattern predicted for different operating conditions has been found to depend on the initial or starting conditions as well as on the ratio of characteristic buoyancy to inertia forces. The latter is called the Archimedes number and is defined by:

$$Ar = \frac{\alpha g \Delta T D}{V_i^2} \qquad (9)$$

where α is the coefficient of thermal expansion, g is the gravitational constant, ΔT is the temperature difference between the outlet and inlet, D is the vessel diameter and V_i is the inlet velocity at the nozzle. In general, two distinct types of flow patterns are predicted, jet-momentum-dominated and buoyancy-dominated. The conditions that can lead to either of these patterns will be discussed by considering steady-state ($\Delta t = 10^{20}$) and transient simulation (Δt = 1 to 5 s) results.

---

* The effective viscosity was set to the laminar viscosity for these cases.

Steady-State Calculations: The first heat addition simulations were done using the steady-state calculation procedure. For these, the buoyancy production/destruction term G_B was set to zero. Two types of runs were made. In the first type, the iteration process was advanced by allowing an isothermal or near-isothermal velocity field to develop (similar to that in Figure 5(a)) before applying the steady-state heat load. This type of run is termed FRactional Heat Load (FRHL). It is similar to an actual reactor start-up procedure in which the moderator pumps are turned on to establish circulation before the reactor is brought to full power. In the second type, the iteration process is initiated with FUll Heat Load (FUHL) and zero internal velocities throughout. Both types of runs are started with the same flow and temperature boundary conditions that, in this case, are characterized by an Archimedes number of 0.25. Figures 6(a) and 6(b) illustrate that the FRHL simulations result in a jet-momentum-dominated flow typified by a large recirculating vortex with downflow in the core region and a relatively cool "hot spot" above the vessel mid-plane. The downflow velocities are significantly higher than for the isothermal case indicating that buoyancy forces tend to enhance recirculation. The FUHL simulation (Figures 7(a) and (b)) results in a buoyancy-dominated flow field, characterized by upflow in the core region and full jet reversal approximately 0.8 RAD from the nozzle outlet. Because of the reversal of the jet, much of the cool incoming liquid flows along the lower part of the reflector region towards the outlet. The normalized temperature field contours indicate a stable stratification in the top half of the vessel with the highest temperature occurring at the top.

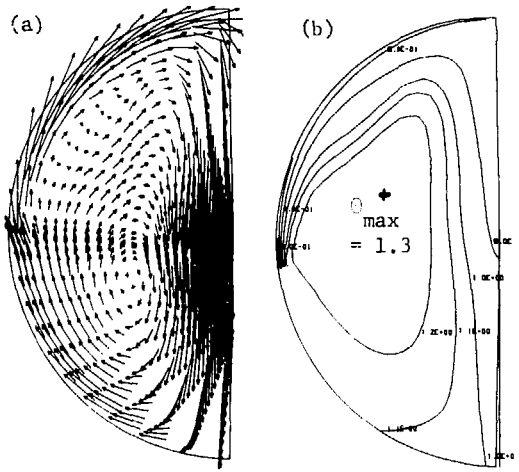

Figure 6

Jet-Momentum-Dominated. (a) Velocity Field, (b) Normalized Temperature Field; Ar = 0.25, G_B = 0.0

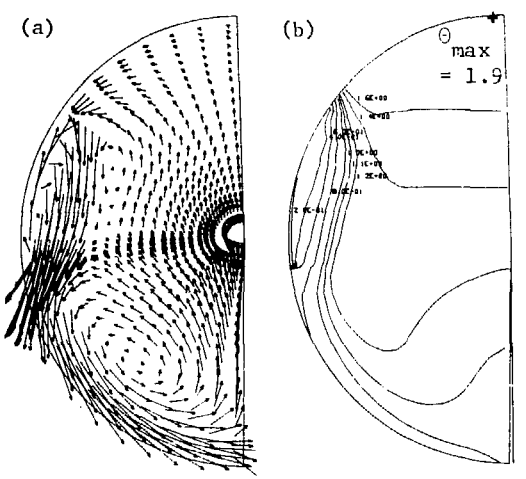

Figure 7

Buoyancy-Dominated. (a) Velocity Field, (b) Normalized Temperature Field, Ar = 0.25, G_B = 0.0

The two distinct flow patterns predicted for the same operating conditions illustrates the importance of the initial or starting conditions to the final solution. The steady-state calculation procedure is unsuitable since it cannot properly account for either the actual rate at which heat is added to the system or the heat capacity of the liquid. These factors can only be properly considered by using a transient calculation procedure.

Transient Calculations: Several transient simulations were performed for operating conditions corresponding to Ar = 0.25, 0.34 and 0.49. These are summarized in Table 2 below.

TABLE 2: SUMMARY OF TRANSIENT SIMULATIONS

RUN NO.	Ar	G_B	INTERNAL VALUES OF u,v,T at t=0	HEAT LOAD HISTORY	INLET FLOW AND TEMPERATURE HISTORY	STEADY-STATE FLOW PATTERN
1	0.25	Zero	u=v=0, $T=T_i$	$Q=Q_{SS}$ for all t	SS values for all t	MD
2	0.25	Zero	u=v=0, $T=T_i$	$Q=Q_{SS}$ for all t	$T=T_i$ for all t; linear increase of flow from 0 at t=0 to SS value at t=60 s	MD
3	0.25	Zero	u=v=0, $T=T_i$	Linear increase of Q from 0 at t=0 to SS level at t=60 s	SS values for all t	MD
4	0.25	Zero	u=v=0, $T=T_a$	$Q=Q_{SS}$ for all t	SS values for all t	MD
5	0.34	Zero	u=v=0, $T=T_i$	$Q=Q_{SS}$ for all t	SS values for all t	BD
6	0.25	Non-zero	u=v=0, $T=T_i$	$Q=Q_{SS}$ for all t	SS values for all t	MD
7	0.34	Non-zero	u=v=0, $T=T_i$	$Q=Q_{SS}$ for all t	SS values for all t	MD
8	0.49	Non-zero	u=v=0, $T=T_i$	$Q=Q_{SS}$ for all t	SS values for all t	BD

SS = steady-state
MD = jet-momentum-dominated
BD = buoyancy-dominated

The first five runs were done with the buoyancy generation/destruction term G_B set to zero. Runs 1 to 4 at Ar = 0.25 were made to investigate the effect of heat load history, inlet flow and temperature history, and initial internal temperature. All of these cases resulted in a jet-momentum-dominated flow pattern at steady-state, identical to the one shown in Figure 6(a) for the FRHL simulation.

After some experimenting it was found that a buoyancy-dominated flow pattern was predicted only when the Archimedes number was increased beyond 0.32. Figure 8 shows the temporal variations of the normalized temperature and circumferential velocity at the top of the vessel for Ar = 0.25 (Run No. 1) and Ar = 0.34 (Run No. 5). The Figure shows that initially the flow is jet-momentum-dominated for both cases*. The flow pattern corresponding to Ar = 0.25 remains momentum-dominated at steady-state. This is indicated by the levelling off of both the velocity and temperature beyond t = 600 s. In contrast, the

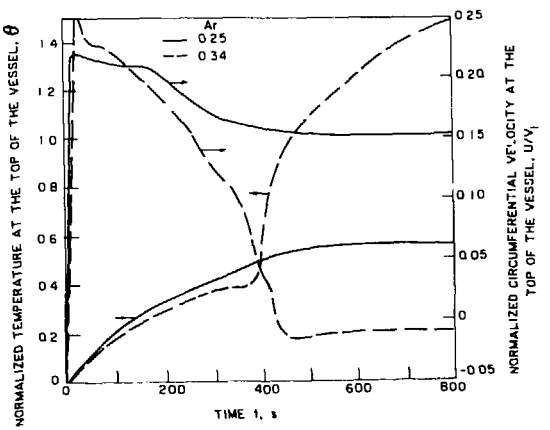

Figure 8

Temporal Variation of Normalized Circumferential Velocity and Temperature at the Top of the Vessel: G_B = 0.0

* The two simulations were continued to t = 1200 s. The final flow and temperature fields were virtually identical to those obtained after t = 800 s for both Archimedes numbers.

circumferential velocity for the Ar = 0.34 case decreases rapidly with increasing time, becoming negative at t $\tilde{=}$ 430 s. This is roughly the point in time at which the core flow switches from downflow to upflow. It is interesting to note the sharp increase in the maximum temperature that takes place before the velocity becomes negative. Figures 9(a) to 9(d) show the evolution of the flow pattern with time for Ar = 0.34. The Figures show that flow reversal begins in the low velocity outer region of the jet and propagates towards the vertical plane of symmetry.

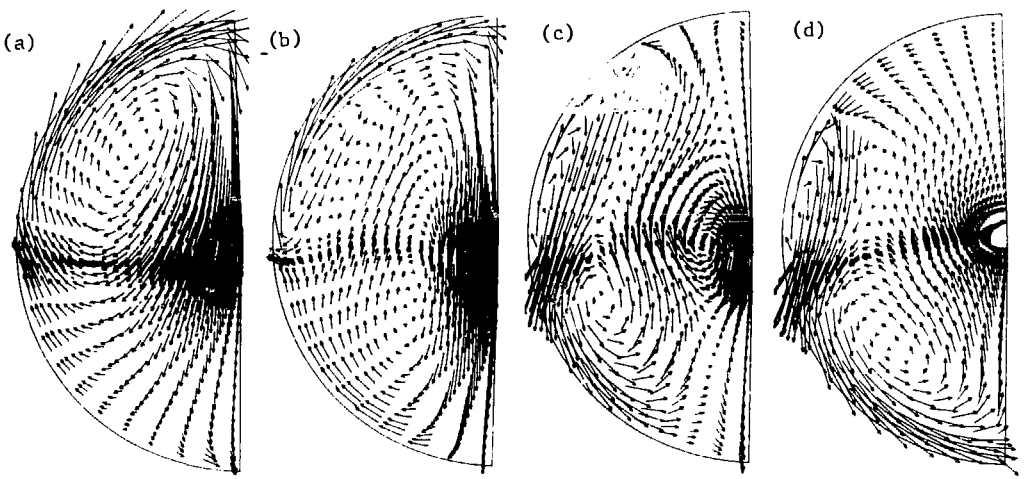

Figure 9
Evolution of Flow Pattern with Time for Ar = 0.34 Simulation: (a) t = 100 s, (b) t = 300 s, (c) t = 400 s, (d) t = 500 s; G_B = 0.0

Runs 6 to 8 were made to investigate the effects of including a buoyancy term in the turbulence model. This was done by defining the turbulence generation/destruction term G_B in terms of the temperature gradient along each coordinate direction (see Table 1). The term is negative for stable stratification (increasing temperature with elevation) and positive otherwise. The effect of buoyancy on turbulence generation/destruction was found to be negligible for the Ar = 0.25 simulation. However, the predicted flow pattern for Ar = 0.34 was jet-momentum-dominated when G_B was non-zero. A buoyancy-dominated flow was predicted only by increasing Ar beyond 0.34. For example, a simulation with Ar = 0.49 (Run 8) results in a buoyancy-dominated flow after about 275 s. The predicted effective viscosities above the mid-plane for this run are 1 to 2 orders of magnitude lower than for Run 5, which was made with G_B set to zero*. The lower effective viscosities result in a lower spreading rate for the jet. This in turn results in an increased capacity for the jet to induce a downflow in the core region. Hence, a jet-momentum-dominated flow can be maintained at higher Archimedes numbers.

CONCLUSIONS

A numerical model has been developed to simulate the two-dimensional moderator flow and temperature distributions in a CANDU reactor vessel. Isothermal flow

* The predicted effective viscosities with G_B set to zero range from 10^{-2} to 10^{-1} $kg \cdot m^{-1} \cdot s^{-1}$ near the walls to 1 to 10 $kg \cdot m^{-1} \cdot s^{-1}$ in the core region. The magnitudes are identical for both jet-momentum- and buoyancy-dominated flows.

predictions are in reasonable agreement with measurements made in a full-scale mock-up. Non-isothermal simulations have been made using both steady-state and transient calculation procedures. In general, depending on the value of the Archimedes number and on initial conditions, two types of flows have been predicted: jet-momentum-dominated and buoyancy-dominated. Transient simulations have indicated that the latter occurs only for relatively high Archimedes numbers. When buoyancy effects on turbulence generation/destruction are modelled, buoyancy-dominated flows are predicted to occur at yet higher Archimedes numbers. This is attributed to the lower effective viscosities predicted near the outer edge of the jet.

NOMENCLATURE

A	= area
Ar	= Archimedes number
a	= finite difference coefficient
C_1, C_2, C_μ	= turbulence model constants
c_p	= specific heat at constant pressure
D	= reactor vessel diameter
F	= frictional force per unit volume
G	= turbulence generation term
g	= gravitational constant
k	= turbulent kinetic energy per unit mass
P	= pressure
p	= center of control volume
Q	= volumetric heat generation rate
r	= radial direction
S	= source term; stagnation point
Su	= volume-integrated source term
t	= time
T	= temperature
u	= circumferential velocity
v	= radial velocity
V	= velocity magnitude
VOL	= cell volume

Greek Symbols

α	= coefficient of thermal-expansion
β	= porosity: fluid-filled volume ÷ total volume
Γ	= exchange coefficient
ε	= turbulence energy dissipation rate per unit mass
Θ	= $(T-T_i)/(T_o-T_i)$, normalized temperature
θ	= circumferential direction
μ	= dynamic viscosity
ρ	= fluid density
σ	= turbulent Prandtl number

Subscripts

B	= buoyancy
i	= inlet
k	= turbulent kinetic energy
n	= nozzle
nb	= neighbouring points
o	= outlet
r	= radial direction, reference
S	= shear
t	= turbulent

ε = energy dissipation rate
θ = circumferential direction
eff = effective

ACKNOWLEDGEMENTS

The author is grateful to the Atomic Energy of Canada Engineering Company for providing financial support for part of this work. Thanks are also due to I. Cheung for her programming assistance and to M. Schwantz for typing the manuscript.

REFERENCES

1. Gosman, A.D., Pun, W.M., 1974, Lecture Notes for Course Entitled: "Calculation of Recirculating Flows", Imperial College, HTFS/74/2.

2. Hepworth, R.D., 1967, Unpublished AECL Report.

3. Patankar, S.V., 1980, Numerical Heat Transfer and Fluid Flow, Hemisphere Publishing Corp.

4. Patankar, S.V., Spalding, D.B., 1972, "A Calculation Procedure for Heat Mass and Momentum Transfer in Three-Dimensional Parabolic Flows", Int. J. Heat and Mass Transfer, Vol. 15, pp. 1787.

5. Rodi, W., 1980, "Turbulence Models for Environmental Problems", Chapter in Prediction Methods for Turbulent Flows , Kollmann, W., Ed., Hemisphere Publishing Corp.